Is Geometry or Dynamics More Important in Cardiac Arrhythmogenesis?

Arun V. Holden, Stephen H. Gilbert, and Alan P. Benson

Institute of Membrane and Systems Biology & Multidisciplinary Cardiovascular Research Institute, University of Leeds, Leeds LS2 9JT, UK
a.v.holden@leeds.ac.uk, s.h.gilbert@leeds.ac.uk, a.p.benson@leeds.ac.uk

Summary. We examine the effects of cardiac geometry and architecture on the excitable media paradigm, and illustrate the effect of cardiac structure on the dynamics of arrhythmias by investigating scroll wave filament dynamics in two biophysically-detailed heterogeneous models of the human left ventricular free wall.

1 Introduction

During ventricular fibrillation (VF), rapid, self-sustained and spatio-temporally highly irregular electrical excitation waves in the ventricles results in loss of their normal synchronised rhythmic beating (Fig. 1). Both experimental [11] and computational [10] evidence supports the idea that VF is sustained by re-entrant wave propagation, in which a wave of excitation propagates through, away from, and back into, the same piece of tissue. Re-entrant waves have been mathematically idealised in extensive homogeneous isotropic excitable media by 2D spiral and 3D scroll waves [17]. Virtual cardiac tissues have proved to be an effective tool for simulating cardiac propagation patterns, and for proposing hypotheses that can be tested experimentally [6]. This excitable medium paradigm provides a simple explanation for the development of monomorphic ventricular tachycardia (VT) into VF: the normal sinus rhythm is a repetitive sequence of wavefronts propagating though the myocardium; a wavebreak leads to VT (analogous to a spiral or scroll wave), which breaks down into the spatio-temporal irregularity of VF. This oversimplified and seductive cartoon is illustrated in Fig. 1, where arrhythmogenesis is explained in terms of wave stability. This reaction diffusion framework has been remarkably successful in providing simple mathematical explanations for arrhythmic behaviours, e.g. meander of spiral waves in terms of Hopf bifurcations [1] and its control by resonant drift [5]. However, it fails to address some details and major problems of the clinical phenomenology. Clinicians talk of substrate for arrhythmias, not as the properties of the cardiac tissue within which arrhythmias occur, but as their heterogeneity.

A.D. Fitt et al. (eds.), *Progress in Industrial Mathematics at ECMI 2008*,
Mathematics in Industry 15, DOI 10.1007/978-3-642-12110-4_53,

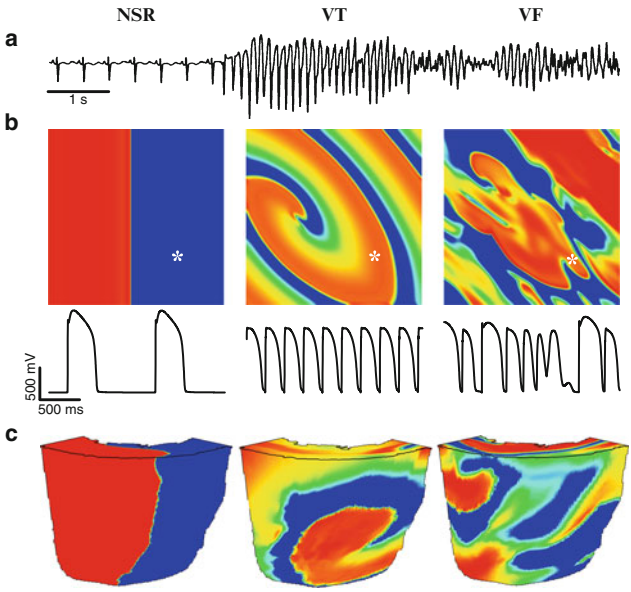

Fig. 1. (**a**) Electrocardiogram showing degeneration into cardiac arrhythmia – from normal sinus rhythm (NSR) to ventricular tachycardia (VT) then ventricular fibrillation (VF). (**b**) In two dimensions, propagation of a continuous wavefront (idealised as a plane wave) represents one excitation of NSR, wavebreak leading to a pair of re-entrant waves (idealised by a single spiral wave) underlies VT, while spatio-temporal irregularity underlies VF. Excited tissue is lighter, resting tissue is darker. Also shown are membrane potential recordings from the sites indicated by asterisks. (**c**) In three-dimensional tissue with orthotropic (fibre and sheet) structure extracted from a diffusion tensor imaged human heart, the qualitative dynamics of propagation underlying the behaviours are the same, but quantitative differences exist

Clinically, re-entrant arrhythmias are more likely to occur when there is an increase in spatial heterogeneity, in either the excitability (dynamics) or coupling (geometry/architecture) components underlying propagation. Heterogeneities in excitability can be mapped by molecular mapping techniques [21], and architectural heterogeneities by diffusion tensor magnetic resonance imaging (DT-MRI) [3]. Mathematically, these heterogeneities emerge as space scales, surface (endo- and epicardial) and internal (scar tissue and blood vessels) boundary conditions, and as spatial changes in excitation and coupling parameters.

2 Ventricular Wall Structural Models

Anisotropic fibre orientation and possible orthotropic sheet structure throughout the ventricular myocardium [9], along with the tissue geometry and heterogeneous cell electrophysiology, underlie both the spatio-temporal pattern

of the spread of electrical excitation, and the mechanical properties. Propagation of electrical activity is orthotropically anisotropic [14], being fastest in the direction of the long axis of the fibre due to the presence of gap junctions that are principally located at the ends of the myocytes, and slowest across any sheet planes due to the small number of muscle branches connecting otherwise electrically-insulated muscle sheets [14, 16]. Contraction of myocytes occurs in the long axis direction and, together with transmural shear along sheet planes, results in transmural thickening and apex-base shortening. In DT-MRI [2], theory suggests that the primary eigenvector of the measured diffusion tensor will be along the predominant direction of myocyte long-axis orientation [13, 15, 18] and that the secondary eigenvector will lie in the cleavage plane between sheets [12].

3 The Human Virtual Ventricular Wall

One possible mechanism for the transition from VT to VF is when a single re-entrant wave of excitation (a scroll wave) that rotates around a phase singularity (a filament) with a high frequency breaks down into multiple wavelets. We used the human ventricular electrophysiology model of Ten Tusscher et al. [19] and constructed two heterogeneous models of the left ventricular free wall in order to investigate the influence of tissue geometry and architecture on filament dynamics: (1) a simple cuboid model with dimensions of $60 \times 60 \times 20\,\text{mm}$, where the fibre direction always pointed parallel to the endocardial and epicardial surfaces and rotated 120° across the ventricular wall at a rate of 6°/mm; and (2) a wedge model with geometry and architecture obtained from a DT-MRI data set of the human ventricles. The wedge dimensions are similar to those of the cuboid. In all cases, we set the diffusion coefficient in the fibre direction to give a conduction velocity for a solitary plane wave of $0.7\,\text{m}\,\text{s}^{-1}$. For isotropic propagation we set the diffusion coefficients in the fibre, sheet and sheet normal directions the same. To introduce fibre orientation we set the diffusion coefficients with the ratio 4:1:1 such that conduction velocity is twice as fast along the fibre as across it, i.e. cylindrically anisotropic. To introduce sheet structure and orthotropic propagation, the diffusion coefficients were set with the ratio 36:9:1 to give a conduction velocity ratio of 6:3:1. For filament tracking and quantification we used the method described by Fenton and Karma [8]. We integrated equations using a Forward Time Centred Space method, with an operator splitting and adaptive time step technique [20] utilising a minimum time step of $\Delta t_{min} = 0.02\,\text{ms}$ and a maximum time step $\Delta T = 0.2\,\text{ms}$. Space steps in the cuboid model were $\Delta x = \Delta y = \Delta z = 0.33\,\text{mm}$. In the wedge model, space steps were $\Delta x = \Delta y = 0.425\,\text{mm}$ and $\Delta z = 0.5\,\text{mm}$ as defined by the DT-MRI dataset, to give approximately 4×10^5 nodes inside the tissue. See [4] for more detailed information on the models.

Figure 2 shows snapshots at $t = 2\,\text{s}$ of membrane potential on the surface of the model geometries and corresponding filament locations, for both models

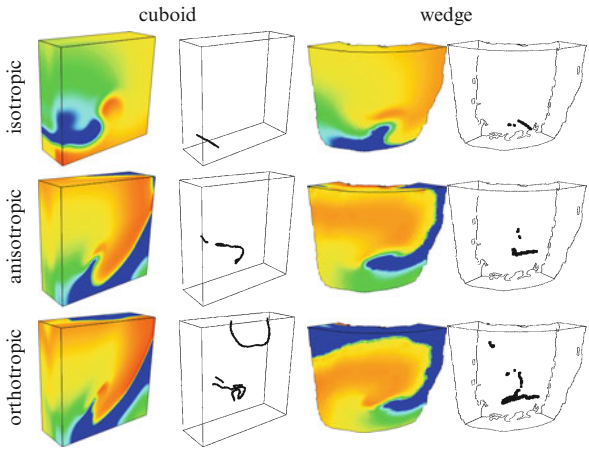

Fig. 2. Snapshots of membrane potential and filament locations after 2 s of re-entrant activity in isotropic, anisotropic and orthotropic cuboid and wedge models. For both models the snapshots are from an epicardial aspect, with the scroll wave rotating clockwise

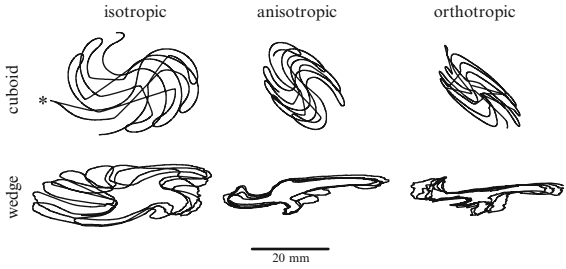

Fig. 3. Filament trajectories on the epicardial surface of the cuboid and wedge models during 1 s of simulation, under isotropic, anisotropic and orthotropic conditions. The asterisk on the isotropic cuboid trajectory indicates where the filament moved off the epicardial surface of the geometry

under isotropic, anisotropic and orthotropic conditions. For the isotropic cuboid, the scroll wave dies out soon after as the filament reaches the boundary. The multiple filaments for the orthotropic cuboid show the beginning of scroll wave breakup – numerous wavelets form soon after and the activation patterns in the tissue represent the complex patterns seen during VF. Note the numerous filaments present in the wedge model under all three conditions. Filament trajectories on the epicardial surfaces of the geometries are shown in Fig. 3. For the cuboid model, changing from isotropy through anisotropy to orthotropy has the effect of rescaling the meander of the filament in the direction perpendicular to the fibre axis, which on the epicardial surface is the sheet normal direction. Scroll wave filament length during 1 s of simulation

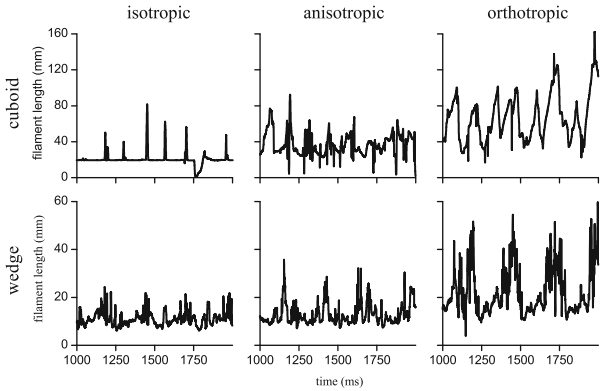

Fig. 4. Scroll wave filament length during 1 s of simulation in the cuboid and wedge models, under isotropic, anisotropic and orthotropic conditions. Note the different scales on the ordinate for the cuboid and wedge models

is shown in Fig. 4. Note the different scales on the ordinate for the cuboid and wedge models. For all conditions, the filament length in the cuboid is longer than in the wedge, a result of tissue geometry (i.e. size) rather than architecture. Oscillations of filament length are evident in all simulations, a consequence of filament twist which is due to the heterogeneous excitation kinetics in the models – see [7]. For both models, filament length increases as anisotropy and then orthotropy are introduced. These effects – due to rotational anisotropy – further increase the effects of the transmural excitation heterogeneity. Although filament curvature increases with anisotropy then orthotropy in the wedge model, the same pattern is not seen in the cuboid. The maximum twist along a single filament increases in both models as anisotropy and then orthotropy are introduced.

4 Conclusions

The normal sinus rhythm of the heart, re-entrant arrhythmias and fibrillation can all be described by the propagation of nonlinear waves in an excitable medium. Physiological and pathological patterns can be explained in terms of nonlinear wave properties – the dependence of velocity on rate by nonlinear dispersion, and breakdown from spatio-temporal patterned activity into irregularity by interactions between waves and by changes in wave stability. However, this emphasis on nonlinear wave dynamics neglects the overall architecture of the heart and its heterogeneities. By combining all these structural (or parametric) heterogeneities into computational models of excitation, propagation can be explored and the resultant functional heterogeneities, that are produced by slow recovery processes, emerge. Although the types of possible wave behaviours follow from the physics of excitable media, the details of the

initiation and subsequent evolution of patterns of excitation in cardiac muscle depends on the details of geometry, anisotropic and orthotropic architecture, and heterogeneities.

Acknowledgements

We thank Drs. Patrick A. Helm and Raimond L. Winslow at the Center for Cardiovascular Bioinformatics and Modeling and Dr Elliot McVeigh at the National Institute of Health for provision of the DT-MRI data sets. This work was supported by the European Union through the Network of Excellence BioSim (contract LHSB-CT-2004-005137), the Dr Hadwen Trust for Humane Research, and the Medical Research Council.

References

1. Barkley, D., Kness, M., Tuckerman, L.S.: Phys. Rev. A **42**, 2489–2492 (1990)
2. Basser, P.J., Mattiello, J., LeBihan, D.: Biophys. J. **66**, 259–267 (1994)
3. Benson, A.P., Gilbert, S.H., Li, P., Newton, S.M., Holden, A.V.: Math. Model. Nat. Phenom. (in press)
4. Benson, A.P., Halley, G., Li, P., Tong, W.C., Holden, A.V.: Chaos **17**, 015105 (2007)
5. Biktashev, V.N., Holden, A.V.: Phys. Lett. A **181**, 216–224 (1993)
6. Biktashev, V.N., Holden, A.V., Mirnov, S.F., Pertsov, A.M., Zaitsev, A.V.: Int. J. Bifurcat. Chaos **9**, 695–704 (1999)
7. Clayton, R.H., Holden, A.V.: Prog. Biophys. Mol. Biol. **85**, 473–499 (2004)
8. Fenton, F., Karma, A.: Chaos **8**, 20–47 (1998)
9. Gilbert, S.H., Benson, A.P., Li, P., Holden, A.V.: Eur. J. Cardiothorac. Surg. **32**, 231–249 (2007)
10. Gray, R.A., Jalife, J., Panfilov, A.V., Baxter, W.T., Cabo, C., Davidenko, J.M., Pertsov, A.M.: Science **270**, 1222–1223 (1995)
11. Gray, R.A., Pertsov, A.M., Jalife, J.: Nature **392**, 75–78 (1998)
12. Helm, P.A., Tseng, H.-J., Younes, L., McVeigh, E.R., Winslow, R.L., Magn. Reson. Med. **54**, 850–859 (2005)
13. Holmes, A.A., Scollan, D.F., Winslow, R.L., Magn. Res. Med. **44**, 157–161 (2000)
14. Hooks, D.A., Trew, M.L., Caldwell, B.J., Sands, G.B., LeGrice, I.J., Smaill, B.H.: Circ. Res. **101**, e103–e112 (2007)
15. Hsu, E.W., Muzikant, A.L., Matulevicius, S.A., Penland, R.C., Henriquez, C.S.: Am. J. Physiol. **274**, H1627–H1634 (1998)
16. LeGrice, I.J., Smaill, B.H., Chai, L.Z., Edgar, S.G., Gavin, J.B., Hunter, P.J.: Am. J. Physiol. **269**, H571–H582 (1995)
17. Panfilov, A.V., Holden, A.V.: Computational Biology of the Heart Wiley, Chichester (1997)
18. Scollan, D.F., Holmes, A., Winslow, R.L., Forder, J.: Am. J. Physiol. **275**, H2308–H2318 (1998)
19. ten Tusscher, K.H.W.J.,, Noble, D., Noble, P.J., Panfilov, A.V., Am. J. Physiol. **286**, H1573–H1589 (2004)
20. Qu, Z., Garfinkel, A.: IEEE Trans. Biomed. Eng. **46**, 1166–1168 (1999)
21. Zhang, H.G., Dobrzynski, H., Holden, A.V., Boyett, M.R.: Lect. Notes Comp. Sci. **2674**, 132–140 (2003)